

Supporting Information for: Self-assembly of 2D membranes from mixtures of hard rods and depleting polymers

Yasheng Yang, Edward Barry, Zvonimir Dogic, and Michael F. Hagan
Department of Physics, Brandeis University, Waltham, MA 02454

I. SURFACE TENSION OF SIMULATED MEMBRANES FROM THE HEIGHT-HEIGHT CORRELATION SPECTRUM

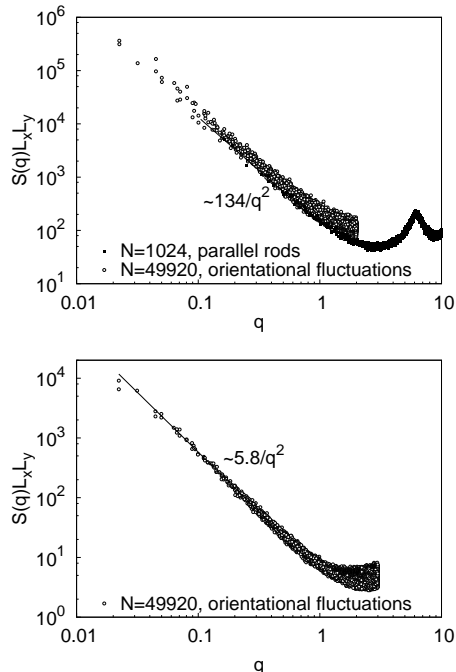


FIG. S1. Height-height correlation spectra for simulated colloidal membranes. (top) Spectra are compared for simulations with a single membrane of $N = 1024$ parallel rods, and a single membrane of $N = 49,220$ rods with orientational fluctuations, with $L = 100$ and $p_s = 0.06$. (bottom) Height-height correlation spectrum for a simulated membrane with orientational fluctuations and parameter values $L = 20$, $p_s = 0.32$, and $N = 49,220$. In all cases $\delta = 1.5$.

We calculate the membrane height-height correlation function (flicker spectrum) of membranes using [1, 2]

$$S(\mathbf{q}) = \langle c_{\mathbf{n}} c_{\mathbf{n}}^* \rangle \quad (1)$$

where \mathbf{q} is the wavevector,

$$\mathbf{q} = 2\pi \left(\frac{n_x}{L_x}, \frac{n_y}{L_y} \right) \quad (2)$$

and the amplitude $c_{\mathbf{n}}$ is given by

$$c_{\mathbf{n}} = \frac{1}{N} \sum_{i=1}^N (z_i - \bar{z}) \exp(-2\pi i(q_x x_i + q_y y_i)) \quad (3)$$

with $\bar{z} \equiv N^{-1} \sum_i z_i$. As shown in Fig. 7 of the main text, the spectrum is proportional to $1/q^2$ at long wavelengths. The effective surface tension σ_{pr} can be extracted from the relation

$$S(\mathbf{q}) = \frac{k_B T}{\sigma_{\text{pr}} L_x L_y q^2} \quad (4)$$

which gives $\sigma_{\text{pr}} \approx 134 k_B T / \sigma^2$ for $\delta = 1.5$, $L = 100$ and $p_s = 0.06$, the case shown in Fig. 7 of the main text. The peak at large q arises from the first peak of radial distribution function shown in Fig. S3.

Fig. S1(top) compares the membrane height-height correlation functions for membranes composed of parallel rods and rods with orientational fluctuations. The calculation details for the height-height correlation spectra are described in section II of the SI^I. We observe that, for all the wavelengths allowed the fluctuation spectrum scales with wave number $1/q^2$ in both cases. For parallel rod membranes this scaling is forced by construction [3]. In contrast for membranes with orientation degrees of freedom rods, $1/q^2$ scaling arises because the large rod aspect ratio of constituent rods leads to a high bending modulus. The q -dependence of the fluctuation spectrum reflects a superposition of bending and protrusion modes, according to $S \sim \frac{k_B T}{\gamma q^2} + \frac{k_B T}{\kappa_c q^4}$ [4], with γ the surface tension and κ_c the bending modulus. The q^4 dependence should dominate for wave numbers smaller than $q_c \cong (\gamma/\kappa_c)^{1/2}$ [4]. We simulated a relatively large membrane of $N = 49,220$ rods to access as small wavevectors as possible, but we observe no sign of q^4 scaling. The large magnitude of the bending modulus can be understood to arise from the large aspect ratio of our rods based on the scaling arguments in Ref. [4]. There it is shown that the bending modulus scales quadratically with membrane thickness; i.e., $\kappa_c \sim L^2$.

To further explore the importance of bending modes, we also calculated spectra for isolated membranes comprised of shorter rods with $L = 20$. For this aspect ratio a large osmotic pressure $p_s = 0.32$ was necessary to stabilize the membrane. These membranes are not stable against stacking (Fig. 4 main text), but a simulation with initial conditions of an isolated membrane remains metastable for all observation times that we considered. Notice that even for these shorter rods there is no evidence of q^4 scaling, indicating that $q_c < 0.02$.

II. SIMULATION DETAILS

The simulations of parallel rods used 4 classes of Monte Carlo moves. (1) The positions of rods were sub-

jected to arbitrary displacements, with a magnitude selected from the uniform distribution $d_\alpha \in (-d_{\max}, d_{\max})$ with $\alpha = x, y, z$ and d_{\max} adjusted before the start of the simulation such that acceptance rates were at least 15%. (2) Rods were subjected to larger magnitude moves in the z direction. Much larger moves are possible in the z direction because of rod ordering. Even larger displacements of the rod in the z direction were enabled by combining the rod displacement with a trial move in which any spheres it overlaps with are moved to the mirror position with respect to the center of the rod's new and old positions. Maximum displacements for these moves were adjusted so that acceptance rates were 50%. (4) Positions of spheres were updated by deleting all current positions, placing N_s spheres with random positions, and deleting any which overlap with a rod. The value N_s is chosen from a Poisson distribution with mean $\rho_{s,\text{bath}}V$. The acceptance rates of sphere-insertion depended solely on the ratio of the free volume (that which is not occluded by rods) and the total volume. (5) Finally, the box size was subjected to rescaling in the xy directions according to $\Delta V \in (-V_{\max}, V_{\max})$; the length in the z direction was fixed. The value V_{\max} was chosen so that the acceptance rates were higher than 15%.

The two classes of rod moves (1) and (2) or performed with equal frequency and sphere position updates and box size rescalings were each attempted approximately every $10N_r$ rod moves. Simulations with orientational fluctuations were performed in a similar manner except that additional trial moves updating rod orientations were implemented using quaternions. The umbrella sampling simulations were run until satisfactory convergence of the free energy profile was achieved.

As an example of the typical amount of simulation required, for $L = 100$, $N_r = 512$, $p_s = 0.09$, $\delta = 1.5$, with initial simulation box dimensions $18 \times 15.5 \times 450$, each umbrella window was run for about 2.5×10^8 sweeps, with a sweep consisting of $5N_r$ random rod displacements, $5N_r$ z rod displacements, a sphere update, and a box rescaling as described above. There were 40 umbrella windows. For random displacements, $d_{\max} = 0.15$ with acceptance rate 23%, for z displacements $d_{\max} = 40 / [\pi\rho_{s,\text{bath}}(\delta + 1)^2]$ with acceptance rate 55%, and for volume scalings $V_{\max} = 40$ with acceptance rate 29%.

III. COLLECTIVE VS. INDIVIDUAL PROTRUSION INTERACTIONS

In this section we compare the relative importance of collective and individual rod protrusions to membrane-membrane interactions. *Independent* rod protrusions can be described by a mean field estimate [5, 6], in which the protrusion of a single rod from a membrane exposed to depletant osmotic pressure p_s incurs a free energy $f_{\text{rod}} = p_s A d$, with A the cross-sectional area of the rod and z the protrusion distance. For uncorrelated protrusion sites the distribution of protrusions obeys an exponential distribution $p_{\text{prot}}(z) \sim \exp(-p_s A z / k_B T)$, with

$p_{\text{prot}}(z)$ the density of rods with ends located a distance z above the mean surface of the membrane. Although protrusions of rods from colloidal membranes were observed by fluorescence [6], it is not possible to directly evaluate $p_{\text{prot}}(z)$ because these experiments labeled only a small fraction of rods and thus could not distinguish collective from individual protrusions. Thus, to evaluate the independent rod expression, we measured the distribution of protrusions in isolated membranes during simulations. The distributions measured for osmotic pressures of $p_s = 0.06$ and 0.12 are compared to exponential distributions in Fig. 6 of the main text. At large z , where $\rho(z)$ is small, it gradually approaches the exponential distribution $\sim \exp(-p_s A z)$, with the excluded area $A = \pi(\sigma + \delta)^2/4$ and σ the rod diameter. However, the protrusion distribution shows significant broadening near the mean surface of the membrane. Small protrusions incur lower free energy costs due to correlations with neighboring rods. Because rods are closely packed in membranes, the volume they exclude to polymers overlaps, and protrusion of one rod results in a smaller excluded volume cost for a neighboring rod to protrude. Based on the fact that the distribution of protrusions is exponential only asymptotically and that an expression for interactions due to collective protrusion undulations fits simulated membrane-membrane repulsions, we conclude that stabilization of colloidal membranes is primarily due to collective protrusion undulations. A density functional theory [7] which does account for correlations between rods predicts the protrusion distribution much more accurately.

IV. THE ORIGINS OF MEMBRANE-MEMBRANE REPULSIVE INTERACTIONS.

In this section we present in more detail the calculation of the origin of the interactions that stabilize membranes against stacking.

For two flat plates, the depletion interaction is linear for small separations $d \leq \delta$, and negligible for $d > \delta$ [8]. However, the equivalent interaction occurs over a significantly longer range for membranes, due to fluctuations of constituent rods. These fluctuations have two effects on membrane-membrane interactions, which can be disentangled by separating the free energy into a depletion term and a term arising from rod protrusions, $f(d) = f_{\text{ex}} + f_{\text{pr}}$. The depletion term is given by $f_{\text{ex}}(d) = p_s \langle v_{\text{ex}}(d) \rangle$, where v_{ex} is the volume excluded to spheres by rods, and $\langle \cdot \rangle$ indicates an ensemble average over configurations at a particular separation d . The excluded volume (per rod) is calculated for each particular system configuration as $v_{\text{ex}} \approx (L_x L_y L_z - N_s / \rho_s) / N$, with N_s the number of polymer spheres for that configuration. The protrusion term can then be calculated as $f_{\text{pr}}(d) = f(d) - f_{\text{ex}}(d)$. As shown in Fig. S2, the ranges of the depletion and protrusion interactions are comparable, and much larger than the sphere diameter. The en-

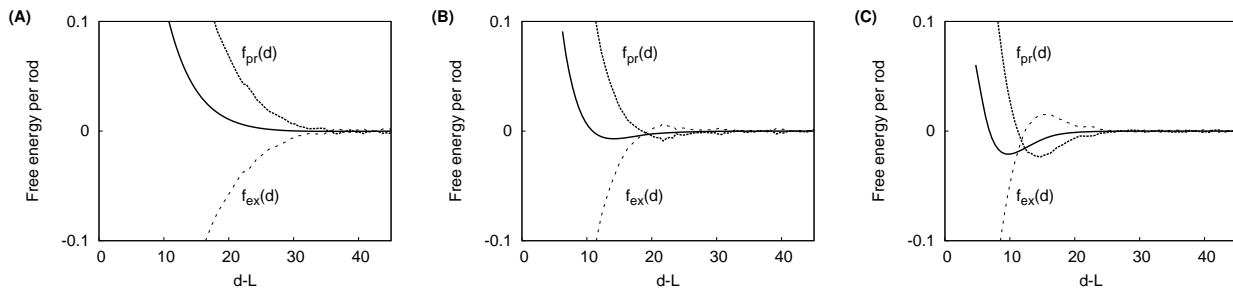


FIG. S2. The total free energy can be split into a depletion term and a term arising from rod protrusions, $f(d) = f_{\text{ex}} + f_{\text{pr}}$. The solid lines are $f(d)$, the dotted lines correspond to the protrusion interaction f_{pr} , and the dashed lines correspond to the depletion interaction f_{ex} . The rod length is $L = 100$, the sphere diameter is $\delta = 1.5$, and osmotic pressures are $p_s = 0.06, 0.09$ and 0.12 , from (A) to (C), respectively.

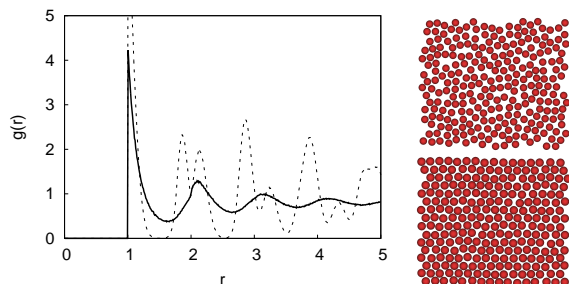


FIG. S3. (Left) Radial distribution functions of rods in the plane of membrane. The membrane is liquid at low surface density (Solid line, $\rho_{2d} = 0.81$ at $p_s = 0.06$), while at high surface density (Dashed line, $\rho_{2d} = 0.98$ at $p_s = 0.12$), a split double peak of $g(r)$ appears at $r \approx 2$ indicating the freezing of the membrane. (Right top) Cross section of a membrane at $p_s = 0.06$. The membrane is a liquid. (Right bottom) Cross section of a membrane at $p_s = 0.12$. The membrane is a solid. Rod length is $L = 100$.

hanced interaction range occurs because membrane undulations bring rods in neighboring membranes within the bare depletion interaction range for large mean membrane separations.

We note that the attractive depletion interactions can expand the range of protrusions as membranes approach, which could result in the lower than expected apparent surface tension measured in Fig. 5 of the main text. For example, for $p_s = 0.12$ in Fig. S2, there is an intermediate distance range $d - L \in [13, 20]$, where $f_{\text{ex}}(d)$ becomes positive; i.e., the excluded volume is larger than the value for membranes with infinite separation, while at the same time the total free energy is lower. At this intermediate distance range, the protrusion susceptibility is increased because the favorable entropy of protrusions is partially offset by partial overlap of excluded volume regions with rods from the opposing membrane. This result emphasizes that the depletion and protrusion forces are intimately coupled in the membrane interaction potential.

V. MEMBRANE CRYSTALLIZATION

As noted in the main text, the simulated membranes crystallize for large osmotic pressures and aspect ratios. Crystallized membranes associate at lower osmotic pressures because they experience lower protrusion free energies f_p . Due to the translational order of rods, two crystallized membranes can approach in such a way that each rod interacts with only one rod in the neighboring membrane. In contrast, when two liquid membranes approach each protruding rod in general interacts with several rods of the neighboring membrane. Consequently, there is a kink in the free energy as a function of osmotic pressure at the point of crystallization, above which the free energy decreases rapidly. We note that our simulations overestimate this effect because crystallized membranes are always aligned with the box directions due to the periodic boundary conditions, which eliminates one rotation required to achieve alignment. Furthermore, we find that larger aspect ratios and/or osmotic pressures are required for membranes to crystallize with orientational fluctuations enabled. Finally, the effect of crystallization on membrane-membrane interaction free energies would be unlikely to be seen experimentally due to kinetic considerations, since large membranes rotate slowly.

The boundary between liquid and crystallized membranes, which is indicated by the dashed line in Fig. 3A of the main text, was determined from radial distribution functions $g(r)$ measured within the plane of membranes at each parameter set; crystallized membranes have a double-peak in the radial distribution function at $r \approx 2$ [9]. Typical examples of $g(r)$ for liquid and crystallized membranes are shown in Fig. S3. The location of the solid-liquid coexistence line can be understood from two-dimensional hard disk systems, which computational studies [10, 11] showed freeze at a areal density $\rho_{2d} \approx 0.88$. The transition in our simulations occurs at an areal rod density of 0.88 ; the relationship between osmotic pressure and areal rod density is theoretically calculated in Ref. [7].

There has been much discussion in the literature concerning the possibility that a hexatic phase precedes

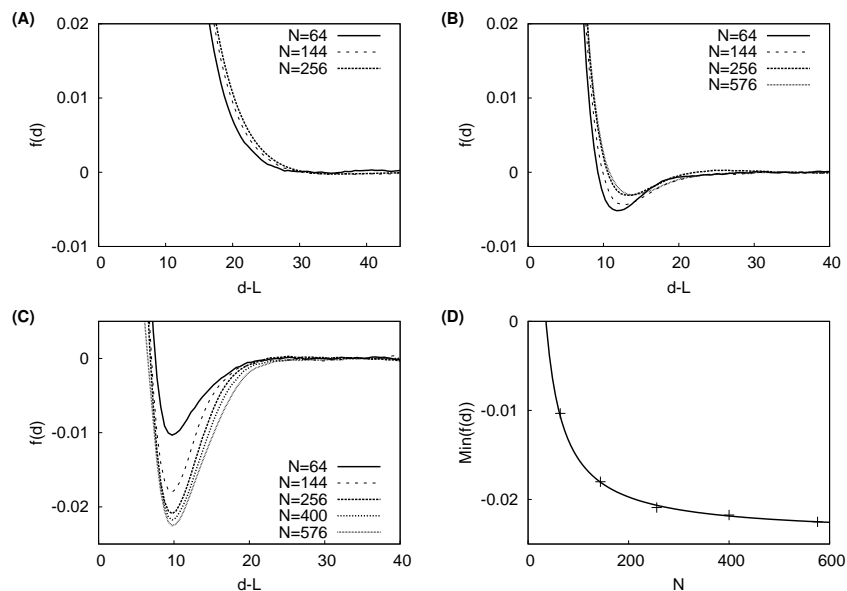


FIG. S4. Evaluation of finite size effects. (A)-(C) The free energy per rod $f(d)$ measured at membrane sizes $N = 64, 144, 256, 400$ and 576 . Parameters are: (A) $L = 100$ and $p_s = 0.06$, for which membranes are repulsive; (B) $L = 50$ and $p_s = 0.12$, for which membranes are attractive but in the liquid phase; (C) $L = 100$ and $p_s = 0.12$, for which membranes are attractive and crystallized. (D) The minima of $f(d)$ plotted in (C) v.s. membrane size N . Symbols are the simulation results. The line is the fit against $\min(f_N - f_\infty) = f_0 + k k_B T / 2N$, with fitting parameters $f_0 = -0.023$ and $k \approx 1.7$.

crystallinity in hard disk systems [12]. The number of rods in our membranes is far too small to investigate this possibility here, so we merely note that we see a direct transition from liquid to crystalline, which is consistent with large simulations of hard disks [9, 13, 14].

VI. FINITE SIZE EFFECTS

Since the phase diagrams are determined from simulations with $N = 256$ rods per membrane, it is important to verify that the phase boundaries are insensitive to N . To this end, we calculated membrane-membrane interaction free energies $f(d)$ as described above at a variety of osmotic pressures and rod lengths for membranes with $N = 64, 144, 256, 400$ and 576 . As shown in Fig. S4 A, for repulsive membranes, the free energy stays repulsive irrespective of membrane sizes, despite stronger repulsion for larger membrane sizes. For attractive liquid membranes, F increases (i.e. the attractive basin gets shallower) with increasing N . For attractive crystallized membranes, F decreases (i.e. the attractive basin gets deeper) with increasing N . However, the calculated isolated-smectic and liquid-solid boundaries are insensitive to system size for $N \geq 144$, justifying our choice of 256 rods per membrane.

The finite size dependence of the interaction free energy of crystallized membranes can be understood as follows. Two crystallized membranes can decrease their protrusion free energy by aligning their hexagonal lattices as described above. This alignment is unfavorable entropically since it restricts one the global translational degree of freedom. This alignment restricts one translational degree of freedom, and thus increases the free energy per rod by a factor $\sim k_B T / 2N$. Indeed, the basin depth for $L = 100$ and $p_s = 0.12$, can be fit against

$$\min(f_N) = f_0 + k k_B T / 2N \quad (5)$$

with factor $k \approx 1.7$, as shown in Fig. S4.

Estimation of finite size effects. An upper bound for the pre-factor k in Eq. 5 can be estimated from the precision with which rods are forced to align as: $k_{\text{bound}} = \ln(A_0/A_1)$, with $A_0 = 1/\rho_{2d}$ the area of unit cell of the lattice, and A_1 is the free area for one rod when its neighbors are fixed at their lattice sites. We calculate $A_1 = 12(\frac{1}{4}dc - \frac{1}{2} \arcsin \frac{c}{2})$, with $d = \sqrt{2/\sqrt{3}\rho_{2d}}$ and $c = \frac{1}{2}(\sqrt{3}b - \sqrt{4 - b^2})$. From simulations with parameters $L = 100$ and $p_s = 0.12$ we measure $\rho_{2d} \approx 0.98$, which gives $k_{\text{bound}} \approx 3.6$. The actual value $k < k_{\text{bound}}$ because rods are not perfectly aligned in optimal membrane configurations and there are regions where rods overlap with multiple partners in the opposing membrane.

[1] W. K. den Otter and W. J. Briels, J. Chem. Phys. **118**, 4712 (2003).

[2] E. S. Boek, W. K. Den Otter, W. J. Briels, and

- D. Iakovlev, *Phil. Trans. R. Soc. Lond. A* **362**, 1625 (2004).
- [3] R. Lipowsky and S. Grothaus, *Europhys. Lett.* **23**, 599 (1993).
- [4] R. Goetz, G. Gompper, and R. Lipowsky, *Phys. Rev. Lett.* **82**, 221 (1999).
- [5] J. N. Israelachvili and H. Wennerstrom, *J. Phys. Chem.* **96**, 520 (1992).
- [6] E. Barry and Z. Dogic, *Proc. Nat. Acad. Sci.* **107**, 10348 (2010).
- [7] Y. Yang and M. F. Hagan, to appear in *Phys. Rev. E*.
- [8] S. Asakura and F. Oosawa, *J. Chem. Phys.* **22**, 1255 (1954).
- [9] T. M. Truskett, S. Torquato, S. Sastry, P. G. Debenedetti, and F. H. Stillinger, *Phys. Rev. E* **58**, 3083 (1998).
- [10] H. Lowen, T. Palberg, and R. Simon, *Phys. Rev. Lett.* **70**, 1557 (1993).
- [11] H. Weber, D. Marx, and K. Binder, *Phys. Rev. B* **51**, 14636 (1995).
- [12] K. J. Strandburg, *Rev. Mod. Phys.* **60**, 161 (1988).
- [13] E. Velasco and L. Mederos, *Phys. Rev. B* **56**, 2432 (1997).
- [14] S. Luding, *Phys. Rev. E* **63**, 042201 (2001).